Correcting for trace gas absorption when retrieving aerosol optical depth from satellite observations of reflected shortwave radiation

Falguni Patadia[1,2], Robert C. Levy[2], Shana Mattoo[2,3]

[1]GESTAR/Morgan State University, Columbia, MD, USA
[2]NASA Goddard Space Flight Center, Greenbelt, MD, USA
[3]SSAI, Lanham, MD, USA

Abstract

Retrieving aerosol optical depth (AOD) from top-of-atmosphere (TOA) satellite-measured radiance requires separating the aerosol signal from the total observed signal. Total TOA radiance includes signal from the underlying surface and from atmospheric constituents such as aerosols, clouds and gases. Multispectral retrieval algorithms, such as the dark-target (DT) algorithm that operates upon the Moderate Resolution Imaging Spectroradiometer (MODIS, onboard Terra and Aqua satellites) and Visible Infrared Imaging Radiometer Suite (VIIRS, onboard Suomi-NPP) sensors, use wavelength bands in "window" regions. However, while small, the gas absorptions in these bands are non-negligible and require correction. In this paper, we use the High-resolution TRANsmission (HITRAN) database and Line-by-Line Radiative Transfer Model (LBLRTM) to derive consistent gas corrections for both MODIS and VIIRS wavelength bands. Absorptions from H_2O, CO_2 and O_3 are considered, as well as other trace gases. Even though MODIS and VIIRS bands are "similar", they are different enough that applying MODIS specific gas corrections to VIIRS observations results in an underestimate of global mean AOD (by 0.01), but with much larger regional AOD biases of up to 0.07. As recent studies are attempting to create a long-term data record by joining multiple satellite datasets, including MODIS and VIIRS, the consistency of gas correction becomes even more crucial.

1. Introduction

Aerosols are fine particles in the atmosphere that scatter and/or absorb incoming solar insolation, and because of this are active players in Earth's energy budget [*IPCC*, 2013]. In addition aerosols affect cloud and precipitation processes [*Denman et al.*, 2007; *Boucher et al*., 2013], and they degrade air quality, contributing to increased morbidity and mortality rates world-wide [*Lim et al*. 2012]. For these reasons characterizing and monitoring aerosol distributions has become a global priority [*Boucher et al.*, 2013].

Satellite aerosol remote sensing allows for the characterization and monitoring of aerosols globally [*Lenoble et al.,* 2013]. Different aerosol remote sensing schemes are applied, depending on the information received by the different satellite sensors [*McCormick et al*., 1979; *Herman et al*., 1997; *Stowe et al.*, 1997;*Tanré et al.*, 1997; *Kaufman et al*., 1997a; *Torres et al.*, 1998; *Veefkind et al*., 1998; *Higurashi and Nakajima*, 1999; *Deuzé et al.,* 1999; *Knapp et al*., 2002; *Martonchik et al*., 1998; *Liu et al*., 2005; *Kahn et al*., 2001; *North et al*., 1999, *Bevan et al*., 2012]. In terms of passive satellite sensors that measure the solar radiation reflected by the Earth-atmosphere system, aerosol remote sensing methods must isolate the information obtained from the interaction of solar radiation with aerosols from the information obtained from all other interactions: reflectance from the surface, scattering from atmospheric molecules and clouds, absorption by atmospheric gases, etc. [*Vermote et al*, 1997]. Thus, characterizing and removing these other sources of information in the satellite signal becomes a fundamental part of the process.

Some of the interactions requiring removal continue to receive considerable attention as new sensors are deployed and new aerosol remote sensing algorithms are derived. These include characterizing the contribution from the surface and masking clouds [*Hutchison et al*., 2008; *Shi*

50 *et al*., 2014;]. Other interactions received much less attention, as these are considered to be well-
51 understood and simple to apply to new situations. These latter ones include molecular scattering
52 and gaseous absorption [*Tanré et al*., 1992; *Vermote et al*., 1997]. However, the requirements on
53 the accuracy of aerosol remote sensing products become tighter as instrument capabilities,
54 calibration and retrieval methods improve. For example, *Hollman et al*., (2013) has recently
55 suggested that to reduce uncertainties on climate, aerosol optical depth (AOD) should be
56 monitored to an accuracy on the order of ±(0.03 + 10%; e.g. GCOS, 2011, GCOS-IP, 2016). The
57 Atmospheric Clouds and ocean Ecosystems (ACE) white paper called for an accuracy of ±(0.02
58 + 10%) [*Starr et al.,* 2010]. To meet such tight criteria, all aspects of traditional aerosol remote
59 sensing methods require re-examination with the objective to reduce uncertainties in the final
60 retrieval, and to assure continuity as the aerosol climate data record is passed from one sensor to
61 the next [*Popp et al*., 2016].

62 In this paper we focus on gaseous absorption. Aerosol retrieval algorithms (*Vermote et*
63 *al*., 1997) tend to use satellite observations taken in wavelength regions where gas absorptions
64 are small. However, while gas absorption is small in these "window" bands, it is not zero. For
65 example, for the 20 nm-wide Moderate Resolution Imaging Spectroradiometer (MODIS) band
66 near 0.55 μm, in the middle of the Chappius region, there is absorption due to ozone. For a US
67 1976 Standard Atmosphere (US76, 1976), with total column ozone of 344 Dobson Units (DU),
68 the gas absorption optical depth (τ^{GAS}) is about 0.03 in this band. This is of similar magnitude to
69 pristine AOD (~0.05), and is equal to the required measurement accuracy (GCOS; 2011, GCOS-
70 IP, 2016). Water vapor, measured as precipitable water vapor (PW or *w*), absorbs as well and
71 introduces even greater uncertainty. For example, the *w* of the US76 standard atmosphere is a
72 modest 1.4 cm, which translates to τ^{GAS} of about 0.025 in the MODIS 2.11 μm band or a τ^{GAS} of

0.05 for a similar-wavelength Visible Infrared Imaging Radiometer Suite (VIIRS) band centered near 2.25 μm. The major difficulty with ozone and water vapor is that the total column burden of these gases varies spatially and temporally over the globe [*Hegglin et al.*, 2014]. Other trace gases, including carbon dioxide and methane, also absorb shortwave radiation in wavelength specific regions. While these gases are more evenly distributed (well-mixed) across the globe, failing to correct for their absorption would also lead to errors in aerosol retrieval.

Different aerosol retrieval algorithms respond to the challenge of gaseous correction differently. Some include all gaseous absorbers and account for the variability of water vapor and ozone [*Levy et al.*, 2013; 2015], while others use a fixed ozone concentration [e.g Thomas et al., 2010; Sayer et al., 2012], and others correct for some gases, but consider the effect of other gases to be negligible [MISR ATBD 09, 2008 : https://eospso.gsfc.nasa.gov/sites/default/files/atbd/atbd-misr-09.pdf]. Few include methane [Levy et al., 2013; 2015]. How does a less complete gaseous correction scheme affect the global retrieval of AOD? How sensitive are gaseous absorption schemes to slight shifts in spectral bands from instrument to instrument? While all operational aerosol retrieval algorithms employ gaseous correction schemes in their retrieval and describe these schemes, more or less, within the "gray literature" of internal documentation, there are few recent articles in the peer-reviewed literature that openly describe the process and quantify the impact of the subtle choices made during algorithm development.

In this paper we re-examine gaseous correction as it is applied in the traditional MODIS Dark Target (DT) aerosol retrieval [*Levy et al*., 2013], and as that retrieval algorithm is ported to the new VIIRS data [*Levy et al*., 2015]. In Section 2 we discuss the absorption of radiation by atmospheric gases within the MODIS and VIIRS bands used for the DT aerosol retrieval. We

introduce the relationship of gas abundance to its transmittance spectra, which is the theoretical basis for gas corrections in DT AOD retrievals. The atmospheric gas correction methodology is detailed in Section 3. The impact of the updated atmospheric gas corrections applied to the Collection 6 MODIS AOD is also briefed in Section 3. In Section 4 we discuss the importance of accurate atmospheric gas corrections in the context of DT AOD retrievals from the VIIRS instrument. The study is summarized and concluded in Section 5.

2. The DT approach to aerosol retrieval and gas correction

2.1 The DT aerosol algorithm and wavelength bands

As explained in detail by Levy et al. (2013; 2015) and references therein, the dark-target (DT) aerosol algorithm uses seven channels (or bands) covering the solar reflective spectral region from blue to the shortwave infrared (SWIR) to characterize aerosols, clouds and the Earth's surface. These bands were specifically chosen to correspond to the spectral window regions of minimal gas absorption. On MODIS, these bands include B1, B2, B3, B4, B5, B6 and B7, which are each 20-50 nm in width and centered near 0.65, 0.86, 0.47, 0.55, 1.24, 1.63 and 2.11 μm, respectively. On VIIRS, the DT algorithm uses bands M3, M4, M5, M7, M8, M10 and M11, which are the "moderate resolution" or M-bands with 20 and 60 nm bandwidths, and are centered near 0.48, 0.55, 0.67, 0.86, 1.24, 1.60 and 2.26 μm, respectively.

The DT algorithm is actually two algorithms, one applied to MODIS- or VIIRS-measured reflectance over land surfaces and the other to measured reflectance over ocean (Levy et al., 2013; 2015). Both the land/ocean algorithms employ a single atmospheric gas correction method before any retrieval is performed. DT uses a LUT approach in which atmospherically corrected

observed top-of-atmosphere (TOA) reflectance is compared with simulated reflectance. The simulations are calculated by radiative transfer codes, and account for multiple scattering and absorption effects of a combined surface (land or water), molecular (Rayleigh), and aerosol scene, but do not account for gaseous absorption. These simulations also account for the angular dependence of the scattered radiation, through use of a pseudo-spherical approximation (e.g. Ahmad and Fraser, 1991). The DT retrieval operates on regions of pixels for which cloud pixels, glint pixels, and other unsuitable pixels have been masked out. Thus, the DT aerosol retrieval is performed for cloud-free sky, and assumptions have been made about the surface reflectance properties and atmospheric constituents. The LUT is interpolated as a function of observing geometry (solar and view zenith and azimuth angles), and then searched to determine which aerosol conditions provide the spectral reflectance that best "matches" the spectral reflectance observed by the satellite. The reported solution (retrieved spectral AOD) is some function of the solutions that meet sufficient criteria for matching the observations. For the DT algorithm, expected uncertainty for retrieved AOD at 0.55 μm (as compared to global network of sun photometers) is ±(0.05 + 15%) over land, and ±(0.03 + 10%) over ocean [*Levy et al.*, 2013].

These LUTs are created as if the atmosphere is composed only of aerosol and scattering (Rayleigh) molecules. The gas absorption is assumed to be zero. This is because of the large spatial/seasonal variability of two of the primary absorbers: ozone and water vapor. Ozone can range from 100 to 500 DU around the globe [*Hegglin et al*. 2014] and water vapor varies by an order of magnitude from the wet tropics to the dry poles. It would be cumbersome and computationally inefficient to add two or more new indices to the LUT and cover the dynamic range of each gas in the LUT calculation.

While gas absorption in these window bands may be small, they are not zero, as described above. Figure 1 shows the TOA transmission spectra (black lines) in the 0.4 – 2.5 μm spectral range in the presence of major gases, including H_2O, O_3, CO_2, CH_4, O_2, N_2O, and CO. The transmission spectra of each gas was calculated using the Line-by-Line Radiative Transfer Model (LBLRTM) code [*Clough et al.*, 1992, 2005] for a nadir viewing geometry and for the US 1976 Standard Atmosphere (US76; 1976). A transmittance of 1.0 indicates that the atmosphere is transparent to incoming solar radiation (insolation) i.e. it is not absorbed in the atmosphere. Overlaid on Fig. 1 are the spectral response functions of the seven MODIS channels (blue curves) and seven VIIRS channels (red curves) used in the DT retrievals. As can be seen from Fig. 1, depending on the wavelength, the atmosphere can be totally transparent to a certain gas and partially opaque to another. For example, in the MODIS 0.62-0.67 μm band (B1), H_2O, O_3, and O_2, absorb radiation while CO_2, N_2O, CO, and CH_4 do not. In the 1.230 – 1.250 μm band (B5), O_2, H_2O and CO_2 are major absorbers while other gases are not. Absorption bands of the major atmospheric gases are listed in Table 1.

Note that there are also wavelength regions that are nearly opaque because of gas absorption. For example, Fig. 1 shows the well-known water vapor absorption within the wavelength region near 1.38 μm. Because of the strong absorption, the 1.38 μm band cannot be used for aerosol retrieval. Yet, this band is very useful for detecting cirrus clouds that would otherwise contaminate a cloud-free aerosol retrieval (Gao et al., 2002). This special case of using absorption information is not discussed further in this paper.

2.2 Derivation of a gas absorption correction

Because the LUT is calculated without gas absorption, an alternative technique must be substituted to account for the effect of the gases in each wavelength. If not, then when the algorithm attempts to match the measured TOA reflectances to the LUT-calculated reflectances the LUT values will be brighter than the measured values for the same amount of aerosol. In the most straightforward sense retrieved AOD, dominated by scattering, will be systematically too low because the retrieval will be searching for a less bright TOA reflectance in the LUT, with less aerosol, to match the observed values. The algorithm deals with this mismatch between measured and LUT reflectance caused by the missing gas absorption in the LUT values by adjusting *the measured* TOA reflectances in each wavelength band, in effect brightening the measurements to better match the values in the LUT.

Figure 1 shows that six gases (H_2O, O_3, CO_2, N_2O, O_2 and CH_4) have absorption lines that fall within the wavelength bands used for the DT aerosol retrieval. Because each window band spans tens of nanometers, every DT channel is affected by at least one gas where the transmittance is less than 1.0.

We have introduced two measures, gas opacity and transmissivity corresponding to the gas absorption optical depth and transmittance. The two parameters are related via,

$$T_\lambda^i = \exp\left(-G^i \tau_\lambda^i\right) \qquad \ldots\ldots\ldots (1)$$

where T_λ^i is the downward transmittance for a particular wavelength band or λ, and for a particular absorbing gas "*i*", and where τ_λ^i is the gas optical depth designated for the particular gas and wavelength and G^i is the airmass factor (or the atmospheric path length i.e. the slant path through the atmosphere) for gas *i*. Equation (1) shows that transmission of light is a function of

182 the airmass factor (G^i) and the gas optical depth (τ_λ^i), and that transmissivity decreases with
183 increasing air mass and increasing gas concentration.
184
185 **2.2.1 Gas optical depth**
186 The gas optical depth, τ_λ^i, represents the spectral integral over the wavelength band, and
187 if the gas concentration was uniform along the path (column), then τ_λ^i would be directly
188 proportional to the loading of gas *i* in the column. Some gases are indeed well-mixed in the
189 atmosphere, but water vapor and ozone are not. These important absorbers exhibit distinctive
190 vertical profiles, as will be discussed in Section 3.1. Note that each individual gas has its own
191 particular absorption efficiency based on its characteristic absorption cross section, and that for
192 the same column concentrations τ_λ^i will be different for different gases. In the absence of a long
193 slant path, and for small gas optical depths ($\tau_\lambda^i << 1.0$), transmission can be estimated by
194 $T_\lambda^i \sim 1 - G^i \tau_\lambda^i$.
195
196 **2.2.2 Airmass factor**
197 The airmass factor, G can be approximated as G=1/cosZ where Z is the zenith angle, for a
198 homogenous (exponential decay) atmosphere, and for small values (near nadir) of a zenith angles
199 Z. This is the flat earth approximation. As Z increases beyond 60°, the air mass factor is more
200 accurately described by spherical shell geometry towards the horizon [Gueymard, 1995], i.e.:

$$G = \sqrt{(r\ cos\ Z)^2 + 2r + 1} - r\cos Z \qquad \ldots\ldots\ldots (2)$$

201 where, $r = R_E / H_{atm}$; R_E = radius of Earth (6371km) and H_{atm} = effective scale height of the
202 atmosphere (approx 9km). This expression accounts for Earth's sphericity and atmospheric

refraction. Differences in computing G are small for Z<70°, but increase to 10% as Z = 84° (the maximum zenith angle allowed within the DT algorithm).

Yet, there are complications. When atmospheric constituents are well-mixed and their concentrations are nearly proportional to altitude within the atmosphere, Eq (2) is sufficient. However, water vapor (concentrated near the surface) and ozone (concentrated in the stratosphere) are not well-mixed in the vertical, having different scale heights. In this layered situation (rather than continuous), there are empirical formulas (e.g. *Kasten and Young*, 1989) that provide slight improvements to the calculation of G assuming spherical geometry. For example, *Gueymard*, [1995] derived the empirical formula

$$G^i = (cosZ + a_{i,1} Z^{a_{i,2}} * \left(a_{i,3} - Z\right)^{a_{i,4}})^{-1} \qquad \ldots\ldots\ldots (3)$$

where $a_{i,j}$ are the coefficients (j=1,4) for gas type i. Thus, G^i varies with gas type and specific profile within the atmosphere. The values of coefficients $a_{i,j}$ can be found in Table 4.1 of *Gueymard*, [1995].

As long as the total gas optical depth is small ($\sum_i \tau_\lambda^i \ll 1.0$), the total transmission of all trace gases is well-approximated by the product of each individual gas (i.e).:

$$T_\lambda^{GAS} = \prod_i T_\lambda^i = \exp\left(\sum_i -G^i \tau_\lambda^i\right) \qquad \ldots\ldots\ldots (4a)$$

The total gas transmissivity defined in Equation (4a) for each wavelength band quantifies the degree to which the measured reflectance will be diminished due to gaseous absorption. In order to match the measured reflectances to those calculated for the LUT, these diminished reflectances have to be "corrected" or brightened. This correction factor is simply the inverse transmissivity, $\tilde{T}$,

$$\tilde{T}_{\lambda}^{GAS} = 1/T_{\lambda}^{GAS} = \exp\left(\sum_{i} G^{i}\tau_{\lambda}^{i}\right), \qquad \ldots\ldots\ldots (4b)$$

which when multiplied with the measured reflectance restores the amount of light absorbed by gases along the one-way path of transmission. Or, given a measured radiance, L_M, the corrected (brightened) radiance L, is simply, $L = L_M * \tilde{T}$.

When observing from a ground-based sun photometer (e.g. AERONET), the correction is straightforward, because the path of transmission traverses the depth of the atmosphere only once. The problem is more complicated for satellite remote sensing, because a satellite measures radiation that has traveled downwards through the atmosphere and then back up to space. We have to calculate a two-way correction factor and G must account for the Z angles of both downward (the solar zenith angle) and upward paths (view zenith). As Z gets large, the vertical profile of the gas (layering) becomes more important.

There are two parameters determining the transmission, T_{λ}^{GAS}, and therefore the correction factor, $\tilde{T}_{\lambda}^{GAS}$, and these are G^{i} and τ_{λ}^{i}. The goal, then, is to parameterize equation 4(a) or 4(b) i.e. the relationship between atmospheric transmission of gas and $G^{i}\tau_{\lambda}^{i}$; taking into consideration the varying gas concentrations and their vertical profiles through the atmosphere, around the globe. Furthermore, the parameterization will be developed to link $\tilde{T}_{\lambda}^{GAS}$ directly to column measures of the gases instead of to the optical depth. This allows the algorithm to bypass calculations of optical depth from inputs of precipitable water vapor (w in cm) and ozone (O in Du), and instead use the inputs directly.

3. Use of LBLRTM to derive gas absorption parameterization

To develop an empirical relationship between atmospheric gas transmission, the airmass factor (G^i) and its optical depth (τ_λ^i), we require a radiative transfer (RT) code that can accurately simulate the gaseous absorption and transmission process in the atmosphere. Among other things, the RT code requires these two pieces of information: (a) the absorption cross-sections and concentration of gas constituent in spectral bands of interest and (b) accurate high-resolution information of the absorption spectra of the relevant gases. The MODIS and/or VIIRS channels widths are on order of 20-50 nm. We require a high-resolution database to capture the fine absorption lines within these bandwidths. To address (a) and (b), we use the Line-By-Line Radiative Transfer Model (LBLRTM) to parameterize equations 4(a) and 4(b) instead of a MODTRAN based RT code. The following section provides details of LBLRTM.

3.1 LBLRTM description

The Line-By-Line Radiative Transfer Model (LBLRTM) is known to be an accurate and flexible radiative transfer model that can be used over the full spectral range from ultraviolet to microwave [Clough et al., 2005]. It uses the High-resolution TRANsmission (HITRAN) molecular absorption database [*Rothman et al.*, 2009] to calculate transmittance and radiance of molecular species. The HITRAN2008 database contains over 2,713,000 lines for 39 different molecules. The spectral resolution of the data is different in different spectral regions and for different species [see *Rothman et al.*, 2009]. For example, for water vapor absorption in the Near IR region, the line resolution is 0.001 cm^{-1} [2.5 – 3.4 μm]. The LBLRTM has been extensively validated against atmospheric radiance spectra [e.g. *Turner et al.*, 2003; *Shephard et al.*, 2009; *Alvarado et al.*, 2013]. Use of the HITRAN database and other attributes of LBLRTM provide spectral radiance calculations with accuracies that are consistent with validation data. Limiting

errors are, in general, attributable to line parameters and line shape. Algorithmic accuracy of LBLRTM is approximately 0.5% and is about five times less than the error associated with line parameters [*Clough et al.*, 2005].

3.2 LBLRTM calculations for MODIS and VIIRS

The LBLRTM model was run for many scenarios representing different combinations of gas vertical profiles, gas concentrations and air mass factors for each type of gas and each of the wavelength bands of interest. Transmissions of the ten important atmospheric gases, viz. H_2O, O_3, O_2, N_2O, NO_2, NO, SO_2, CO_2, CO, and CH_4, that affect either the MODIS or the VIIRS spectral bands [*Levy et al*., 2013] were calculated. However, only H_2O, O_3, CO_2, N_2O , O_2 and CH_4 were found to have some absorption in the wavelength bands used for the DT aerosol retrieval (Tables 2.1, 2.2). The results link transmission, T_λ^i , or gas correction factor, $\tilde{T}_\lambda^i$, to gas path length, $G^{H_2O}w$ or $G^{O_3}O$, for water vapor (H_2O) and ozone (O_3), respectively, where w is the precipitable water vapor in cm and O is ozone column loading in DU. Values for w and O are input into the algorithm from ancillary data. The other gases are considered to be well-mixed and not varying spatially or temporally, and therefore, are not dependent on input ancillary data. The final parameterization will be curve fits through the scatter of the model results.

As described in Section 2.2, $\tilde{T}_\lambda^{GAS}$ will be affected by the vertical distribution of the gases in the column, especially at oblique zenith angles. To account for this effect in building the parameterization we use 52 atmospheric profiles (personal communication, Pubu Ciren, NOAA, Chevallier, 2002) that were obtained from model runs, and characterize different locations and seasons (Figure 2). The columnar gas concentrations differ across the 52 profiles, varying by more than a factor of ten for water vapor, and by 100% for ozone. Except for NO_2, which is

highly variable in both horizontal and vertical, the other trace gases tend to be well-mixed throughout the atmosphere. Using radiative transfer calculations, Ahmad et al., (2007) show that NO_2 has largest impact (1%) on TOA reflectance in the blue channels (412 and 443 nm). Other visible channels are impacted to a lesser degree. We will use the term 'dry gas' to denote the eight gases that are neither H_2O or O_3, and use the US 1976 Standard Atmosphere (US 76) as a default profile.

For H_2O and O_3, and each of their respective profiles, we use LBLRTM to calculate air mass factors and transmissions for 10 values of viewing zenith angle, ranging from 0° – 80°. Transmission is integrated across the wavelength band, and weighted by relative sensor response (RSR) (Barnes et al., 1998; Xiaoxiong et al., 2005) within the band. Because air mass factor (G^i) varies with gas type (on account of the vertical profile), LBLRTM calculates G^i as well as transmission for the given column amount of gas *i*. For "dry gas", the integrated RSR weighted transmission is converted to gas optical depth, so dry gas transmission (as a function of air mass factors) is easily computed using Eq (1). The US 1976 Standard Atmosphere (US 76) profiles are used to compute "dry gas" transmission for nadir view.

Figure 3 plots the relationship between absorption correction factor, $\tilde{T}_\lambda^{GAS}$, and gas path length, $G^{H2O}w$, for H_2O (panel a) and, $G^{O3}O$, for O_3 (panel b), for MODIS. Figure 4 plots the same for VIIRS. These correction factors (inverse of transmission) are plotted for each window band, for different combinations of H_2O or O_3 concentrations (*w* in cm or *O* in DU) and internally derived air mass factors (G^i) for the given gas type and specific vertical profile. Water vapor, being so variable as well as concentrated near the boundary layer, cannot be explained with a linear relationship. However, for water vapor (panels (a) in both figures 3, 4), a near-

linear dependence of $\tilde{T}_{\lambda}^{H_2O}$ to $G^{H2O}w$ does exist in log-log space. Although, even within the log-log space, there is a small curvature that required a quadratic empirical fit. For ozone, however, the log of our correction factor ($\tilde{T}_{\lambda}^{O_3}$) is nearly linear as a function of absorption through a slant path ($G^{O3}O$). Again, note that G^{i} is computed by LBLRTM, and represents the curvature and vertical profile of each gas type.

Equation 5 describes the quadratic empirical relationship (seen in Fig.3a and Fig 4a) between the gas transmission correction factor of water vapor ($\tilde{T}_{\lambda}^{H_2O}$), its concentration ($w$) and air mass factor ($G^{H2O}$):

$$\tilde{T}_{\lambda}^{H_2O} = \exp\left(\exp\left(K_{1,\lambda}^{H_2O} + K_{2,\lambda}^{H_2O}\ln(G^{H_2O}w) + K_{3,\lambda}^{H_2O}(\ln(G^{H_2O}w))^2\right)\right) \quad \ldots\ldots\ldots(5)$$

and Equation 6 describes the near linear relationship for ozone (panels b in both Fig. 3 and Fig. 4).

$$\tilde{T}_{\lambda}^{O_3} = \exp\left(K_{1,\lambda}^{O_3} + K_{2,\lambda}^{O_3}(G^{O_3}O)\right) \quad \ldots\ldots\ldots(6)$$

"O" denotes ozone concentration in Eq. 6 and G^{O_3} is the airmass factor for Ozone and is computed using equation 3.

The regression coefficients $K_{1,\lambda}^{H_2O}, K_{1,\lambda}^{H_2O}, K_{1,\lambda}^{H_2O}$ and $K_{1,\lambda}^{O_3}, K_{2,\lambda}^{O_3}$ (the slopes and intercepts) for H_2O and O_3 are presented for MODIS and VIIRS in Tables 3.1 and Table 3.2. The slope and intercepts are wavelength dependent (lines of different color on Figs. 3 and 4) and in accordance with absorption characteristics of the gas. For example Table 2.1 shows that water vapor

absorption is the highest in MODIS band 7 (B7 = 2.11 μm) and lowest in B3 (0.47 μm). Correspondingly, the slope and intercept for the H_2O regression relation (Table 3.1) indicates largest water vapor correction in B7 and lowest in B3. Similarly, largest correction (and slope) for ozone is in MODIS B4 (0.55 μm) and lowest in B7.

To calculate the correction factors for water vapor ($\tilde{T}_\lambda^{H_2O}$) and ozone ($\tilde{T}_\lambda^{O_3}$), Equations (5) and (6) require information on water vapor (w) and ozone concentration (O). For the DT algorithm, these are provided by an ancillary data set. For the current version (e.g. MODIS Collection 6), ancillary data are acquired from National Center for Environmental Prediction (NCEP) analysis, specifically the "PWAT" and the ozone fields from the 1° X 1° global meteorological analysis (created every six hours – format "gdas.PGrbF00.YYMMDD.HHz"). Note that there are water vapor products derived operationally from MODIS and VIIRS data (e.g. Gao and Goetz, 1990; Kaufman and Gao, 1992). However, the DT aerosol algorithm runs before these other algorithms in the processing chain, causing the internally-derived water vapor to be unavailable to the aerosol algorithm in real-time processing and thus, the reliance on ancillary data.

In case the ancillary information is not available, the gas absorption can still be estimated. Either a forecast field (e.g. GDAS forecast) or a "climatology" can be used. For example, if the US76 atmosphere is assumed as the climatology for gas profiles, then τ^i for that gas is given in Table 3.1 and 3.2. In this case, we use Equations (7) and (8) to calculate correction factors for water vapor and ozone respectively:

$$\tilde{T}_\lambda^{H_2O} = \exp\left(G^{H_2O}\,\overline{\tau^{H_2O}}\right) \quad \ldots\ldots\ldots (7)$$

$$\tilde{T}_\lambda^{O_3} = \exp\left(G^{O_3}\,\overline{\tau^{O_3}}\right) \quad \ldots\ldots\ldots (8)$$

where $\overline{\tau^{H_2O}}$ and $\overline{\tau^{O_3}}$ are the climatological mean values of gas optical depth for water vapor and ozone, respectively.

$\tilde{T}_{\lambda}^{Dry\ Gas}$ is the correction factor due to dry gas, which includes CO_2, CO, N_2O, NO_2, NO, CH_4, O_2, SO_2, and other trace gases in LBLRTM calculations. For the DT retrieval bands only CO_2, N_2O, CH_4, O_2 contribute to absorption (Tables 2.1, 2.2). Since the gases are generally well-mixed throughout the entire atmosphere and do not experience day-to-day changes, we only consider the climatological mean of the total optical depth of the combined dry gases, and compute its transmittance factor as follows:

$$\tilde{T}_{\lambda}^{Dry\ Gas} = \exp\left(G^{i}\overline{\tau^{Dry\ Gas}}\right) \quad \ldots\ldots\ldots (9)$$

Fig. 5 presents the gas optical depth for a US76 atmosphere, for the MODIS bands and corresponding VIIRS bands. In some cases, (e.g. B4 vs. M5) the differences are small. In other cases (e.g. B5 vs. M8), the total optical depth may be similar, but the relative contribution between different gases is different. Finally, in at least one set of bands (B7 vs. M11), both the total optical depth and the relative contributions between gases is very different. The US76 is a case with a small amount of water vapor (w=1.4 cm), but one can see how quadrupling the w (e.g. as in a tropical atmosphere) would greatly change the relative correction needed for B7 vs. M11, or even B1 vs. M5.

3.3 Application within the DT algorithm.

Whether using "climatology" for water vapor and ozone columns, or using the estimates from a meteorological assimilation system (e.g. GDAS for the current DT algorithm), we need to

correct for the combined absorption of all gases. The total gas absorption correction term, $\tilde{T}_{\lambda}^{gas}$, is the product of individual gas corrections, that is

$$\tilde{T}_{\lambda}^{gas} = \tilde{T}_{\lambda}^{H_2O}\tilde{T}_{\lambda}^{O_3}\tilde{T}_{\lambda}^{Dry\ Gas} \ldots\ldots\ldots (10)$$

The MODIS DT aerosol retrieval algorithm ingests calibrated and geolocated MODIS-measured reflectance data, known as the Level 1B (L1B) product. The corresponding VIIRS DT algorithm ingests a similar VIIRS-measured product. This measured reflectance, (ρ_{λ}^{L1B}), is corrected for atmospheric water vapor, ozone and dry gas, using the correction factors derived above for each wavelength band:

$$\rho_{\lambda} = \tilde{T}_{\lambda}^{gas}\rho_{\lambda}^{L1B} \ldots\ldots\ldots (11)$$

where ρ_{λ} is the corrected or brightened reflectance that can now be used to compare with the calculated TOA reflectances of the LUT, as described in Section 2.2. Note that this spectral reflectance ρ_{λ}, represents the combination of Rayleigh (molecular scattering), plus aerosol in the atmosphere. It also includes contributions from Earth's surface (land or water).

The gas-absorption correction methodology is the same whether performed for MODIS or VIIRS. In fact, the equations (Eqs 5-11) have remained the same throughout all versions of the DT algorithm. As our ability to characterize absorption lines as well as the spectral response of the sensor has improved, it is the coefficients of the equations that have evolved. When the DT algorithm was updated from Collection 5 (C5) to Collection 6 (C6), the underlying gas absorption corrections became more sophisticated (Levy et al., 2013). This is represented in Table 4. The primary differences between C5 and C6 are that the HITRAN database in LBLRTM is used in C6 instead of the MODTRAN parameterization available in 6S that was used in C5, and that additional "dry" gases have been included in C6's correction. These changes

made a difference. The latest version of aerosol data from DT is Collection 6.1 that uses the same gas absorption corrections as C6. As the DT algorithm is ported from MODIS to VIIRS data, the quality of gas correction will also make a difference.

4 Impact of new gas coefficients

The DT retrieval is based on a LUT approach wherein the measured and modeled spectral reflectance is matched for inversion. Any change affecting the calculation of gas-corrected spectral reflectance will subsequently affect the retrieved AOD. *Levy et al.*, [2013] showed the impact of using the updated atmospheric gas corrections on MODIS C6 AOD retrievals. This led to higher AODs globally. Over land (ocean), the 0.55 μm global mean AOD differed by ~0.02 (0.007). The large (>0.02 regionally) change over land was primarily due to a larger gas correction in the 1.24 μm MODIS B5 band (see *Levy et al.*, 2013; Fig. A2), which in turn increased the reflectance in B5, and the subsequent estimate of the NDVI in the SWIR channels (B5 vs. B7) used to estimate surface reflectance in other bands (Levy et al., 2010). The stronger gas correction in B5 came from including the O_2 absorption, which had not been accounted for in C5 (see Table 2.1). Interestingly, Levy et al. [2013] noted that while the overall correction in B7 (2.11 μm) remained similar, the relative weightings of "dry gas" and H_2O was revised.

Even though the MODIS and VIIRS instruments have similar channels, the MODIS gas correction coefficients cannot be applied to aerosol retrievals from VIIRS observations. The slight differences in the bandwidth and channel's central wavelengths (See Fig. 5) will compromise the accuracy of aerosol retrievals. For example, as compared with MODIS B7 (2.11 μm), the VIIRS M11 (2.25 μm) band has less absorption from H_2O. However, MODIS B7 lies in a CO_2 absorption band, while VIIRS M11 lies in a region of CH_4 absorption. Although the CH_4

412 optical depth in VIIRS M11 is small (~0.03), it will affect the dark-target retrievals in the same
413 way as O_2 inclusion affected C6 retrievals (when compared to C5).

414 As a perturbation experiment we intentionally apply the MODIS gas corrections to the
415 VIIRS observations, even though we know this to be incorrect. Figure 6a plots the spatial
416 distribution of spectral TOA reflectance after applying VIIRS-appropriate gas corrections. It
417 shows the mean monthly TOA reflectance for VIIRS. Figure 6b are the reflectance differences
418 between applying VIIRS-appropriate gas corrections and MODIS gas corrections to VIIRS
419 observations. From top to bottom, we find a mean difference of 0%, -0.5%, -6.6%, -2.7%, -
420 1.5%, 3.2% and 5.3% respectively in VIIRS channels M3, M4, M5, M7, M8, M10, M11.
421 Looking back at Fig. 5, one can see that for example, by using proper M5 assumptions instead of
422 the B1 MODIS assumptions, we now apply only about half the correction as before, resulting in
423 a 6.6% reduction of reflectance. Channel M7, with about 50% less water vapor correction (see
424 Fig. 5), results in 2.7% lower reflectance. Larger gas corrections owing to CO_2 absorption in
425 M10 and CH_4 absorption in M11 (Fig. 5), result in positive bias in M10 and M11 reflectance
426 values globally.

427 Now, we continue the perturbation experiment and test the impact of slight differences in
428 the band positioning between MODIS and VIIRS on AOD retrieval by performing two sets of
429 retrievals. The first set (a) is if we applied appropriate VIIRS band corrections, while the second
430 (b) is as if we had simply (naively) applied MODIS (C6) coefficients to VIIRS data. Figure 7
431 shows the AOD retrieved from these two cases (panels a and b) for an entire month (July 2013)
432 of VIIRS data. While general AOD spatial patterns are in agreement, panel (c) shows differences
433 in AOD of up to 0.07 between the two retrievals. Clearly, naively applied MODIS gas
434 corrections to VIIRS data, would lead to a global mean AOD underestimate of ~0.01 for July

435 2013. While these differences are within the global uncertainties for AOD (e.g. GCOS), the
436 regional differences can be much larger.

437 Although once considered to be trivial in magnitude, accurate atmospheric gas
438 corrections have become more important as we strive towards better accuracies in AOD products
439 and towards a seamless climate data record. It is noteworthy that the gas absorption spectra of
440 Figure 1 have been updated several times in recent years [Alvarado et al. 2012] as the scientific
441 community continues to engage in study of gas absorption lines with improved instrumentation
442 and gas spectroscopic measurements. Changing gas absorption spectra will affect the channels
443 designed for new remote sensing instruments and in understanding how these lines might affect
444 the retrieval of proposed geo-physical products. Every instrument design involves
445 characterization of channel bandwidths and the spectral response functions of the instrument's
446 channels. This aptly calls for updates in modeling the absorption by gases in the channels used
447 for aerosol retrievals. For the MODIS Collection 6 AOD product, the team switched from using
448 a MODTRAN gas spectroscopic database to the HITRAN spectroscopic database and found
449 differences.

450 **5. Summary and Conclusions**

451 Performing aerosol optical depth retrieval, from satellite measurements, requires
452 extracting the aerosol signal from the total radiance measured by the sensor at the top-of-
453 atmosphere. The total radiance includes signal from the underlying surface and from atmospheric
454 constituents such as gases, clouds and aerosols. In this paper, we have described the physics and
455 methodology employed by the Dark-Target aerosol retrieval algorithm for atmospheric gas
456 correction of the cloud-free radiance measurements from the MODIS and VIIRS sensors. We

457 have shown that the empirical correction applied to one sensor (MODIS) cannot be applied to
458 another sensor (VIIRS) even when the channels of the two sensors may be similar. For a specific
459 month of VIIRS observations (July, 2013), not accounting for the sensor's bandwidth and
460 positioning of its central wavelength in the electro-magnetic spectrum, can result in an AOD
461 retrieval bias of about 0.01 (global average) and up to 0.07 at regional scales.

462 Water vapor, ozone and carbon dioxide are the major absorbers of solar radiation.
463 Historically, they have been accounted for in atmospheric gas corrections by aerosol retrieval
464 algorithms. However, until recently, standard routine algorithms (e.g. the DT algorithm used on
465 MODIS) did not consider other gases. For example, oxygen with a gas optical depth of about
466 0.016 is important in the MODIS Band 5 (1.24 μm) [Levy et al., 2013]. Methane is an important
467 absorber in band M11 (2.25 μm) of VIIRS with an optical depth of ~0.05. Starting with MODIS
468 Collection 6, and the DT algorithm ported to VIIRS, three additional atmospheric gases [N_2O,
469 CH_4, O_2, SO_2] are addressed by the gas correction in these DT algorithms.

470 For the 'dry gas' component, the DT gas correction assumes a homogeneous global
471 distribution spatially and a US76 type of vertical distribution for the eight gases. Carbon dioxide,
472 oxygen, nitrous oxide and methane are major absorbers in our 'dry gas' category. Except for
473 NO_2, which is highly variable in both horizontal and vertical, the other gases tend to be well-
474 mixed throughout the atmosphere. Spatial variability of well-mixed gases is typically around
475 10%, mostly latitudinal and is smaller than seasonal variability (e.g. see methane maps here:
476 http://www.temis.nl/climate/methane.html). For the nadir view, 10% error due to spatial
477 variability will only introduce an error of 0.005 in the methane correction (optical depth ~0.05 in
478 VIIRS channel M11). For now, this is a small uncertainty in the overall retrieval. However, as
479 requirements for aerosol retrieval accuracies tighten, even these well-mixed dry gases will

480 require removal of any seasonal and regional biases by using ancillary measurements of these
481 gases or at least seasonal global climatology of gas optical depths, instead of a single
482 climatological value for the entire globe.

483 Since the DT algorithm corrects for H_2O and O_3 using ancillary data at every 1˚ X 1˚ grid
484 box, spatial and seasonal variability of these gases is being accounted for. However, the ancillary
485 data has its own uncertainties that propagate into the gas correction and aerosol retrieval. The
486 Dark-Target team is working towards estimating the error in per-pixel AOD retrievals introduced
487 from several error sources including the errors in H_2O and O_3 ancillary data (GDAS) used for
488 atmospheric gas corrections. Preliminary analysis suggests (not shown here) that gas corrections
489 errors, stemming from considering 20% errors in ancillary data, are much smaller (more than an
490 order of magnitude) than errors from surface albedo uncertainty, aerosol model selection, spatial
491 heterogeneity in a scene, calibration and cloud contamination errors. This is work in progress and
492 subject to future publication.

493 The VIIRS instrument onboard Suomi-NPP is a follow-on of the MODIS instrument on
494 Terra and Aqua satellites. While the Dark-Target team strives to create a seamless climate data
495 record (CDR) of AOD from MODIS and VIIRS, it requires a consistency in AOD retrieval of
496 about 0.02. Any compromise with the accuracy of AOD retrieved from either sensor will impact
497 the CDR consistency requirement. To strive toward these requirements, we cannot ignore quality
498 atmospheric gas corrections in AOD retrievals and we will update the gas correction factors for
499 each instrument as the community updates the gas absorption database.

500 As we move into an era of new aerosol missions, revisiting and updating gas corrections
501 in state-of-art algorithm becomes as important as improving upon other factors (e.g. better
502 surface characterization, cloud clearing, aerosol properties etc.) that affect the AOD retrieval.

503 The dark-target algorithm software has now been generalized to retrieve AOD from sensors
504 other than MODIS and VIIRS. It will be necessary to accurately characterize gases from such
505 current and future instruments as Himawari, GOES-R, etc.
506
507
508

Acknowledgements

This research work is funded under NASA's grants for MODIS and VIIRS Dark Target aerosol retrieval for the MODIS science team. We are thankful to Matthew J. Alvarado (from Atmospheric and Environmental Research) for promptly helping with all our queries related to the LBLRTM. We thank Pubu Ciren for providing us with the atmospheric profiles for gases and for knowledge transfer on its use in LBLRTM for calculating NOAA VIIRS atmospheric gas corrections in aerosol retreivals. We thank Dr Lorraine Remer for providing us with scientific comments and for editing the paper.

References

Anderson, G.P., A. Berk, P.K. Acharya, L.S. Bernstein, S.M. Adler-Golden, J. Lee, and L. Muratov, "Reformulated Atmospheric Band Model Method for Modeling Atmospheric Propagation at Arbitrarily Fine Spectral Resolution and Expanded Capabilities," U.S. Patent #7593835, issued September 22, 2009.

Berk, A., G.P. Anderson, P.K. Acharya, L.S. Bernstein, L. Muratov, J. Lee, M. Fox, S.M. Adler-Golden, J.H. Chetwynd, M.L. Hoke, R.B Lockwood, J.A. Gardner, T.W. Cooley, C.C. Borel, P.E. Lewis and E.P. Shettle, "MODTRAN5: 2006 Update," Proc. SPIE, Vol. 6233, 62331F, 2006.

Berk, A., P.K. Acharya, L.S. Bernstein, G.P. Anderson, P. Lewis, J.H. Chetwynd, M.L. Hoke, "Band Model Method for Modeling Atmospheric Propagation at Arbitrarily Fine Spectral Resolution," U.S. Patent #7433806, issued October 7, 2008.

Bevan, S. L., Peter R.J. North, Sietse O. Los, William M.F. Grey, 2012, A global dataset of atmospheric aerosol optical depth and surface reflectance from AATSR, *Remote Sensing of Environment*, 116, 199-210, https://doi.org/10.1016/j.rse.2011.05.024.

Boucher, O., D. Randall, P. Artaxo, C. Bretherton, G. Feingold, P. Forster, V.-M. Kerminen, Y. Kondo, H. Liao, U. Lohmann, P. Rasch, S.K. Satheesh, S. Sherwood, B. Stevens and X.Y. Zhang, 2013: Clouds and Aerosols. In: Climate Change 2013: The Physical Science Basis. Contribution of Working Group I to the Fifth Assessment Report of the Intergovernmental Panel on Climate Change [Stocker, T.F., D. Qin, G.-K. Plattner, M. Tignor, S.K. Allen, J. Boschung, A. Nauels, Y. Xia, V. Bex and P.M. Midgley (eds.)]. Cambridge University Press, Cambridge, United Kingdom and New York, NY, USA.

Charlson, R.J., S.E. Schwartz, J.M. Hales, R.D. Cess, J.A. Coakley, Jr., J.E. Hansen, and D.J. Hoffman, 1992: Climate forcing by anthropogenic aerosols. *Science*, **255**, 423-430, doi:10.1126/science.255.5043.423.

Chevallier, F, 2002, "Sampled database of 60-level atmospheric profiles from the ECMWF analyses", *NWP SAF Report No. NWPSAF-EC-TR-001.*

Clough, S. A., Iacono, M. J., and Moncet, J.-L.: Line-by-Line calculations of atmospheric fluxes and cooling rates: application to water vapor, J. Geophys. Res.-Atmos., 97, 15761, doi:10.1029/92JD01419, 1992.

Clough, S. A., Shephard, M. W., Mlawer, E. J., Delamere, J. S., Iacono, M. J., Cady-Pereira, K., Boukabara, S., and Brown, P. D.: Atmospheric radiative transfer modeling: a summary of the AER codes, J. Quant. Spectrosc. Ra., 91, 233–244, doi:10.1016/j.jqsrt.2004.05.058, 2005.

Denman, K. L., et al., 2007: Couplings between changes in the climate system and biogeochemistry. In: Climate Change 2007: The Physical Science Basis. Contribution of Working Group I to the Fourth Assessment Report of the Intergovernmental Panel on Climate Change [Solomon, S., D. Qin, M. Manning, Z. Chen, M. Marquis, K. B. Averyt, M. Tignor and

H. L. Miller (eds.)] Cambridge University Press, Cambridge, United Kingdom and New York, NY, USA, pp. 499- 587.

Deuzé, J. L., M. Herman, P. Goloub, D. Tanré, and A. Marchand, "Characterization of aerosols over ocean from POLDER/ADEOS-1", Geophys. Res. Lett., 26:10 (1999), 1421–1424.

Gao, B. C., and Alexander F. H. Goetz, Column Atmospheric Water Vapor and Vegetation Liquid Water Retrievals From Airborne Imaging Spectrometer Data, J. Geophys. Res., 95, 3549-3564, 1990.

Gao, B-C., Y. J. Kaufman, D. Tanré, and R-R. Li, 2002: Distinguishing tropospheric aerosols from thin cirrus clouds for improved aerosol retrievals using the ratio of 1.38-μm and 1.24-μm channels. *Geophys. Res. Lett.*, **29.**1890, doi:10.1029/2002GL015475.

GCOS: Systematic observation requirements for satellite-based products for climate, 2011 update, WMO GCOS Rep. 154, New York, USA, 127 pp., 2011.

GCOS-IP 2016: GCOS Implementation Plan 2016. GCOS-200. Available at https://library.wmo.int/opac/doc_num.php?explnum_id=3417

Gueymard, C.: SMARTS2: a simple model of the atmospheric radiative transfer of sunshine: algorithms and performance assess- ment, Florida Solar Energy Center, 1–78, 1995.

Hegglin, M.I. et al. (2014): "Twenty questions and answers about the ozone layer: 2014 Update", in Scientific Assessment of Ozone Depletion: 2014. World Meteorological Organization Global Ozone Research and Monitoring Project - Report No. 55. Available from NOAA ESRL at http://www.esrl.noaa.gov/csd/assessments/ozone/2014/twentyquestions/

Herman, J. R., P. K. Bhartia, O. Torres, C. Hsu, C. Seftor, and E. Celarier, "Global distribution of UV-absorbing aerosols from Nimbus 7/TOMS data", J. Geophys. Res., 102 (1997), 16,911–16,922.

Higurashi, A., and T. Nakajima, "Development of a two channel aerosol retrieval algorithm on global scale using NOAA AVHRR", J. Atmos. Sci., 56 (1999), 924–941.

Hollmann, R., Merchant, C. J., Saunders, R., Downy, C., Buchwitz, M., Cazenave, A., Chuvieco, E., Defourny, P., de Leeuw, G., Forsberg, R., Holzer-Popp, T., Paul, F., Sandven, S., Sathyendranath, S., van Roozendael, M., and Wagner, W.: The ESA Climate Change Initia- tive: satellite data records for essential climate variables, B. Am. Meteorol. Soc., 94, 1541– 1552, doi:10.1175/BAMS-D-11-00254.1, 2013.

Kahn, R., P. Banerjee, and D. McDonald, "The sensitivity of multiangle imaging to natural mixtures of aerosols over ocean", J. Geophys. Res., 106 (2001),18,219−18,238.

Kaufman, Y. J., and B.-C. Gao, Remote sensing of water vapor in the near IR from EOS/MODIS, IEEE Trans. Geosci. Remote Sensing,, 30, 871-884, 1992.

Kaufman, Y. J., D. Tanré, L. A. Remer, E. F. Vermote, A. Chu, and B. N. Holben,"Operational remote sensing of tropospheric aerosol over land from EOS moderate resolution imaging spectroradiometer", J. Geophys. Res., 102, D14 (1997a), 17,051–17,067.

Kaufman, Y. J., A. E. Wald, L. A. Remer, B.-C. Gao, R.-R. Li, and L. Flynn, 1997b: The MODIS 2.1 μm Channel - Correlation with visible reflectance for use in remote sensing of aerosol. *IEEE Trans. Geo*, **35**, 1286-1298.

Kaufman, Y. J., Remer, L. A., Tanré, D., Li, R.-R., Kleidman, R. G., Mattoo, S., Levy, R., Eck, T., Holben, B. N., Ichoku, C., Martins, J. V. and Koren, I.: A critical examination of the residual cloud contamination and diurnal sampling effects on MODIS estimates of aerosol over ocean., *IEEE Trans. Geosci. Remote Sens*., **43**, 2886-2897, 2005.

Knapp, K. R., T. H. Vonder Haar, and Y. J. Kaufman, "Aerosol optical depth retrieval from GOES-8: Uncertainty study and retrieval validation over South America", J. Geophys. Res., 107, D7 (2002), 4055, doi: 10.1029/2001JD000505.

Lenoble, J., L.A. Remer and D. Tanré: Aerosol Remote Sensing, Springer, Heidelberg-New York-Dordrecht-London, 390 pp., ISBN 978-3-642-17724-8, 2013.

Levy, R. C., Mattoo, S., Munchak, L. A., Remer, L. A., Sayer, A. M., Patadia, F., and Hsu, N. C.: The Collection 6 MODIS aerosol products over land and ocean, Atmos. Meas. Tech., 6, 2989-3034, https://doi.org/10.5194/amt-6-2989-2013, 2013.

Levy, R. C., Munchak, L. A., Mattoo, S., Patadia, F., Remer, L. A., and Holz, R. E.: Towards a long-term global aerosol optical depth record: applying a consistent aerosol retrieval algorithm to MODIS and VIIRS-observed reflectance, Atmos. Meas. Tech., 8, 4083-4110, https://doi.org/10.5194/amt-8-4083-2015, 2015.

Li, R.-R., Remer, L., Kaufman, Y. J., Mattoo, S., Gao, B.-C. and Vermote, E.: Snow and ice mask for the MODIS aerosol products., *IEEE Geosci Rem. Sens. Lett*., **2**, 306-310, 2005.

Lim, S. S., et al. (2012), A comparative risk assessment of burden of disease and injury attributable to 67 risk factors and risk factor clusters in 21 regions, 1990?2010: a systematic analysis for the Global Burden of Disease Study 2010, *The Lancet*, *380*(9859), 2224-2260.

Liu, Z., A. H. Omar, Y. Hu, M. A. Vaughan, and D. M. Winker, CALIOP Algorithm Theoretical Basis Document Part 3: Scene Classification Algorithms, PC-SCI-202 Part 3, NASA Langley Research Center, Hampton VA, 2005.

Martins, J. V., D. Tanré, L. A. Remer, Y. J. Kaufman, S. Mattoo and R. Levy , 2002: MODIS Cloud Screening for Remote Sensing of Aerosol over Oceans using Spatial Variability. *Geophys. Res. Lett.*, **29(12)**, 10.1029/2001GL013205, 2002**.**

Martonchik, J. V., D. J. Diner, R. A. Kahn, T. P. Ackerman, M. E. Verstraete, B. Pinty, and H. R. Gordon, "Techniques for the retrieval of aerosol properties over land and ocean using multiangle imaging", IEEE Trans. Geosci. Rem. Sens., 36 (1998), 1212−1227.

McCormick, M. P., P. Hamill, T. J. Pepin, W. P. Chu, T. J. Swissler, and L. R. McMaster, "Satellite studies of the stratospheric aerosol", Bull. Am. Meteorol. Soc., 60 (1979), 1038−1046.

MISR-ATBD-09 , 2008: https://eospso.gsfc.nasa.gov/sites/default/files/atbd/atbd-misr-09.pdf

North, P.R.J., S.A. Briggs, S.E. Plummer, J.J. Settle, 1999, Retrieval of land surface bidirectional reflectance and aerosol opacity from ATSR-2 multiangle imagery, IEEE Transactions on Geoscience and Remote Sensing, 37, 526-537

Popp, et al., Development, Production and Evaluation of Aerosol Climate Data Records from European Satellite Observations (Aerosol_cci), Remote Sensing, 8, 421, 2016; doi:10.3390/rs8050421

Rothman, L. S., et al. (2009), The HITRAN 2008 molecular spectroscopic database, J. Quant. Spectrosc. Radiat. Transfer, 110, 533–572

Sayer, A. M., N. C. Hsu, C. Bettenhausen, Z. Ahmad, B. N. Holben, A. Smirnov, G. E. Thomas, and J. Zhang (2012), SeaWiFS Ocean Aerosol Retrieval (SOAR): Algorithm, validation, and comparison with other data sets, J. Geophys. Res., 117, D03206, doi:10.1029/2011JD016599.

Starr, D. et al.: 2010: Aerosol, Clouds and Ecosystems (ACE) Study Report. Submitted to NASA Headquarters June 2010. https://acemission.gsfc.nasa.gov/documents/Draft_ACE_Report2010%20.pdf

Stowe, L. L., A. M. Ignatov, and R. R. Singh, "Development, validation, and potential enhancements to the second-generation operational aerosol product at the National Environmental Satellite, Data, and Information Service of the National Oceanic and Atmospheric Administration", J. Geophys. Res., 102 (1997), 16,923–16,934.

Tanré, D., B.N. Holben and Y.J. Kaufman, 1992: Atmospheric correction against algorithm for NOAA-AVHRR products: theory and application. *IEEE Trans. Geosci. Rem. Sens*., 30, 231 – 248,doi:10.1109/36.134074.

Tanré, D., Y. J. Kaufman, M. Herman, and S. Mattoo, "Remote sensing of aerosol properties over oceans using the MODIS/EOS spectral radiances", J. Geophys. Res., 102: D14 (1997), 16,971–16,988.

Thomas, G. E., Poulsen, C. A., Siddans, R., Sayer, A. M., Carboni, E., Marsh, S. H., Dean, S. M., Grainger, R. G., and Lawrence, B. N.: Validation of the GRAPE single view aerosol retrieval

693 for ATSR-2 and insights into the long term global AOD trend over the ocean, Atmos. Chem.
694 Phys., 10, 4849-4866, https://doi.org/10.5194/acp-10-4849-2010, 2010.
695
696 Torres, O., P. K. Bhartia, J. R. Herman, Z. Ahmad, and J. Gleason, "Derivation of aerosol
697 properties from satellite measurements of backscattered ultraviolet radiation: Theoretical
698 basis", J. Geophys. Res., 103 (1998), 17,099−17,110.
699
700 U.S. Standard Atmosphere, 1976, U.S. Government Printing Office, Washington, D.C., 1976
701
702 Veefkind, J. P., G. de Leeuw, and P. A. Durkee, "Retrieval of aerosol optical depth over
703 land using two–angle view satellite radiometry during TARFOX", Geophys. Res. Lett.,
704 25:16 (1998), 3135–3138.
705
706 Vermote, E. F., D. Tanré, J. L. Deuzé, M. Herman, and J. J. Morcrette, "Second simulation of the
707 satellite signal in the solar spectrum, 6S: An overview", IEEE Trans. Geosci.Rem. Sens., 35
708 (1997), 675−686.
709
710 W. L. Barnes, T. S. Pagano, V. V. Salomonson, "Pre-launch characteristics of the Moderate
711 Resolution Imaging Spectroradiometer (MODIS) on EOS AM-1", *IEEE Trans. Geosci. Remote*
712 *Sens.*, vol. 36, no. 4, pp. 1088-1100, Jul. 1998.
713
714 Xiaoxiong Xiong, Nianzeng Che and W. Barnes, "Terra MODIS on-orbit spatial characterization
715 and performance," in *IEEE Transactions on Geoscience and Remote Sensing*, vol. 43, no. 2, pp.
716 355-365, Feb. 2005.
717 doi: 10.1109/TGRS.2004.840643
718
719 Z. Ahmad, C. McClain, J. Herman, B. Franz, E. Kwiatkowska, W. Robinson, E. Bucsela, and M.
720 Tzortziou, "Atmospheric correction for NO2 absorption in retrieving water-leaving reflectances
721 from the SeaWiFS and MODIS measurements," Appl. Opt. 46, 6504-6512 (2007).
722
723
724
725
726
727
728
729
730
731
732
733
734
735
736
737
738

Figures

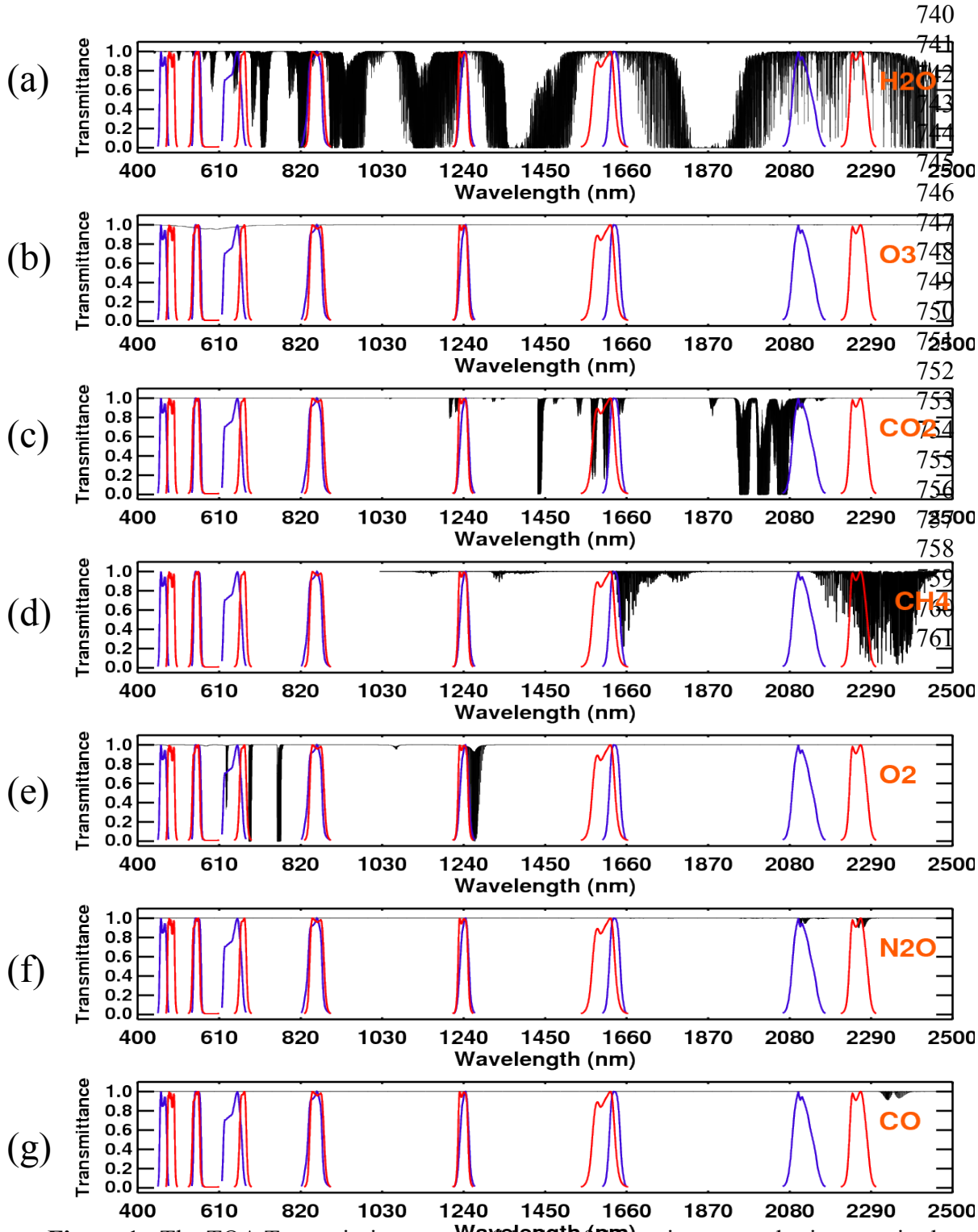

Figure 1 : The TOA Transmission spectra (black) of the major atmospheric gases in the Visible and Near Infrared part of electromagnetic spectrum (400 – 2500 nm). The Line-by-line radiative transfer model (LBLRTM) was used to calculate these gas spectra for a nadir viewing geometry and the 1976 US Standard atmosphere. The spectral response functions of MODIS channels B1-B7 (blue curves) and seven VIIRS channels (red curves) are overlaid to visualize their position in the atmospheric 'window' regions where gas absorption effect is minimal

762

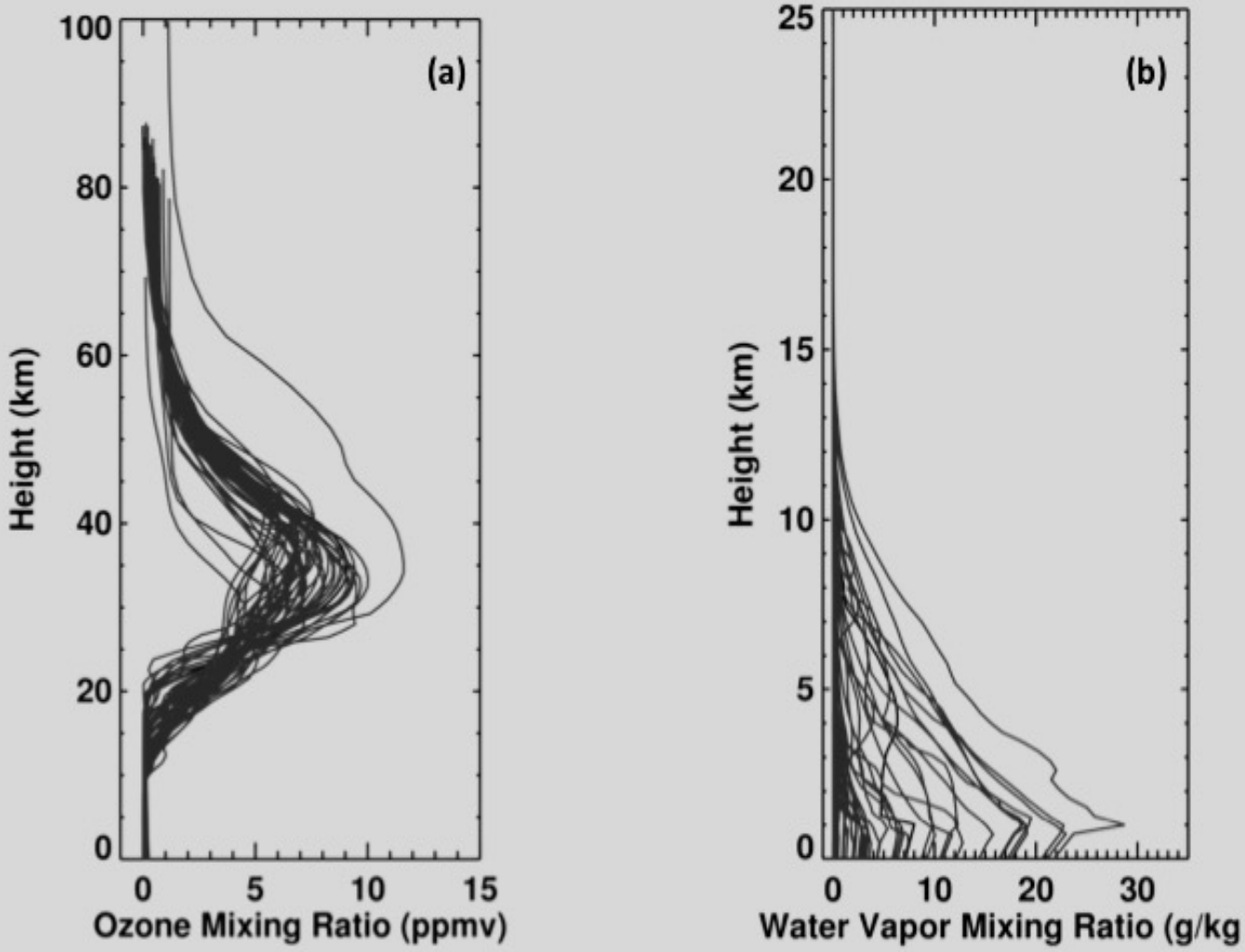

Figure 2: 52 different ECMWF profiles for (a) water vapor and (b) ozone used in the Line-by-line radiative transfer model to calculate the respective gas transmittance.

763
764
765
766
767
768
769
770

771

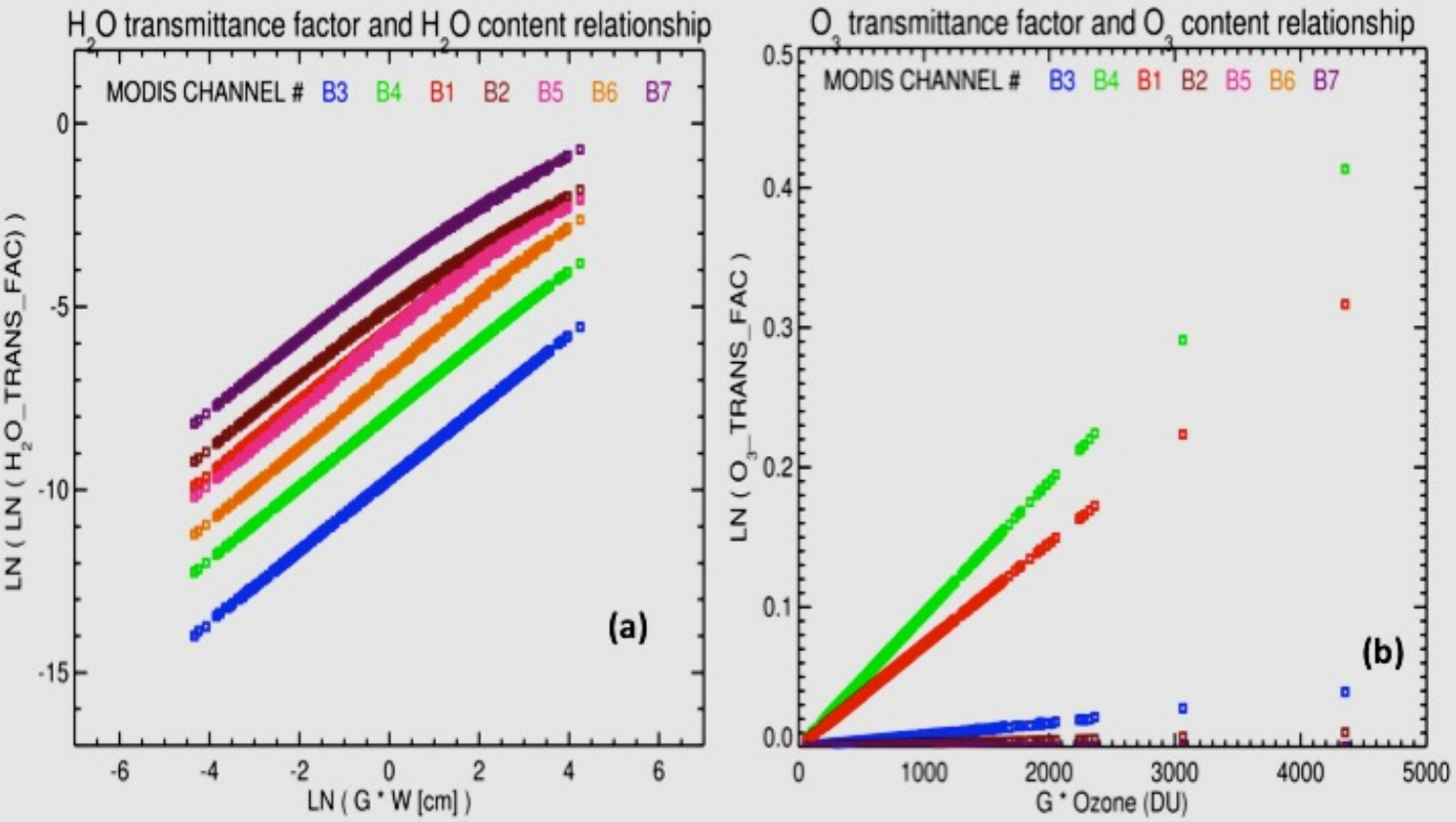

Figure 3: Relationship between Gas Transmittance factor and Gas Content in the MODIS channels B1 – B7 : (a) For H_2O and (b) for O_3. Gas content is scaled by the airmass factor [G]

772
773
774
775
776
777
778
779
780
781
782
783

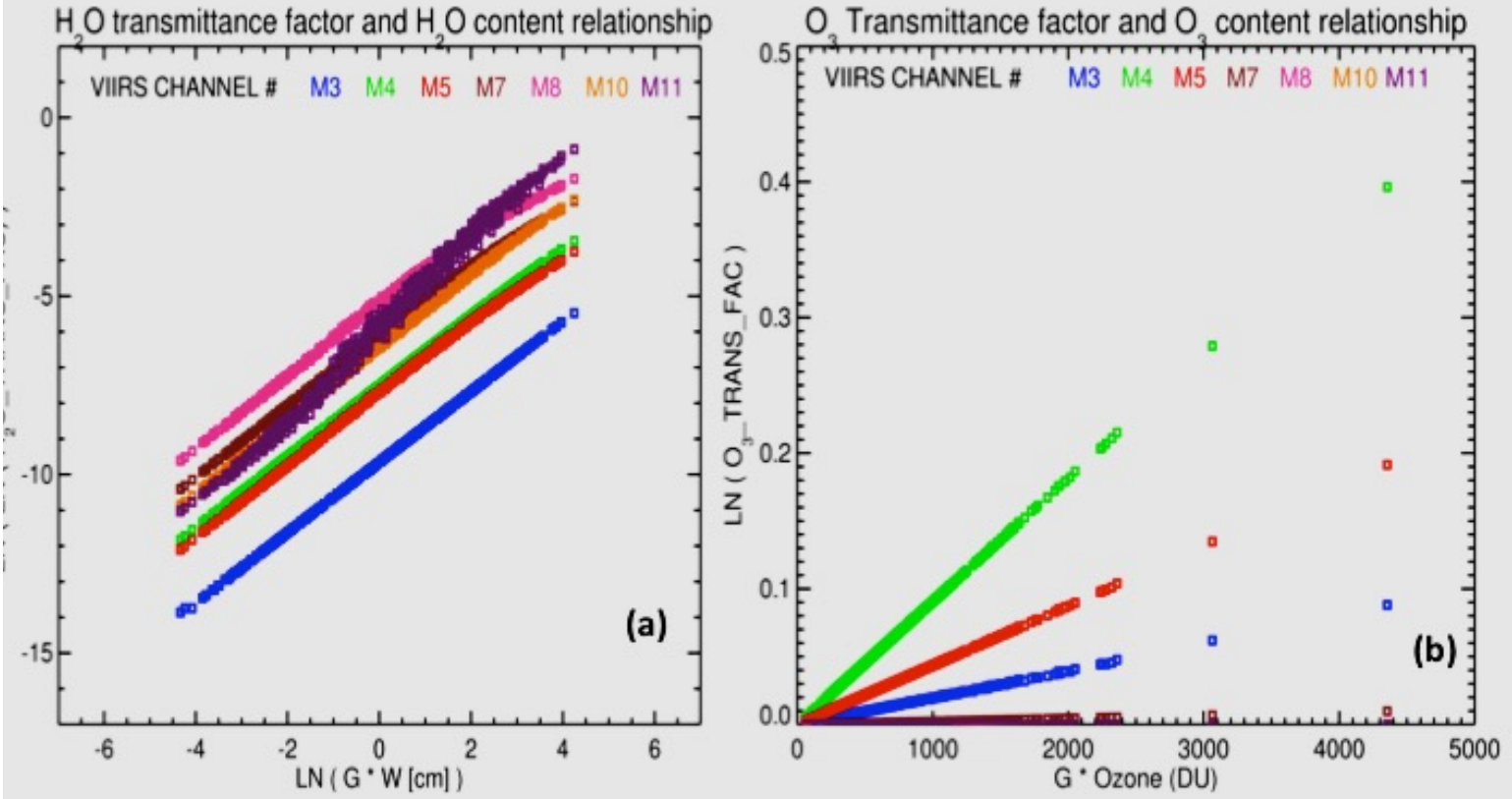

Figure 4: Relationship between Gas Transmittance factor and Gas Content in the seven VIIRS channels: (a) For H_2O and (b) for O_3 Gas content is scaled by the airmass factor [G]

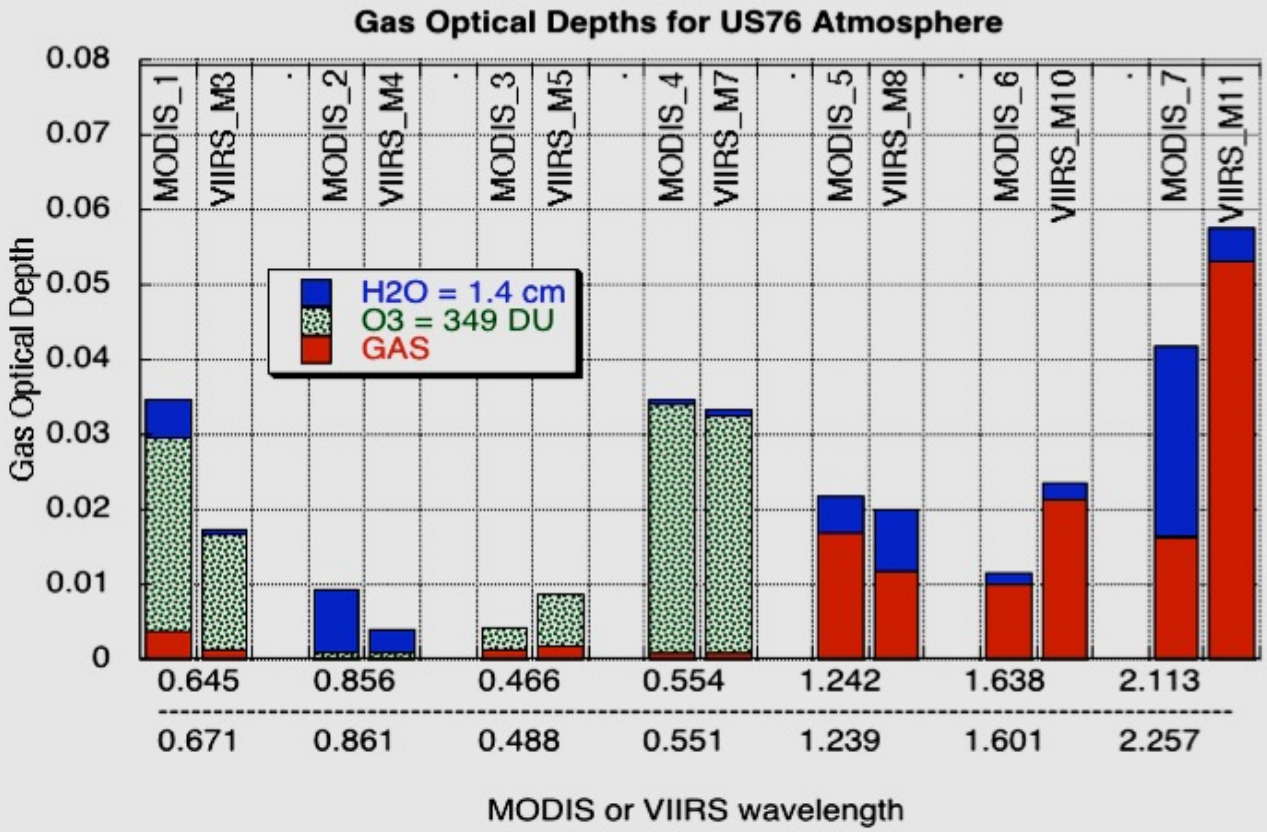

Figure 5 : Comparison of gas optical depths calculated for US 1976 standard atmosphere using MODIS C6 and VIIRS gas correction coefficients. Different colors represent constituent gases (H_2O = blue, O_3 = green hatched, 'dry' gas = red . Large differences in gas optical depths are seen in MODIS Channels 1, 2,6 & 7.

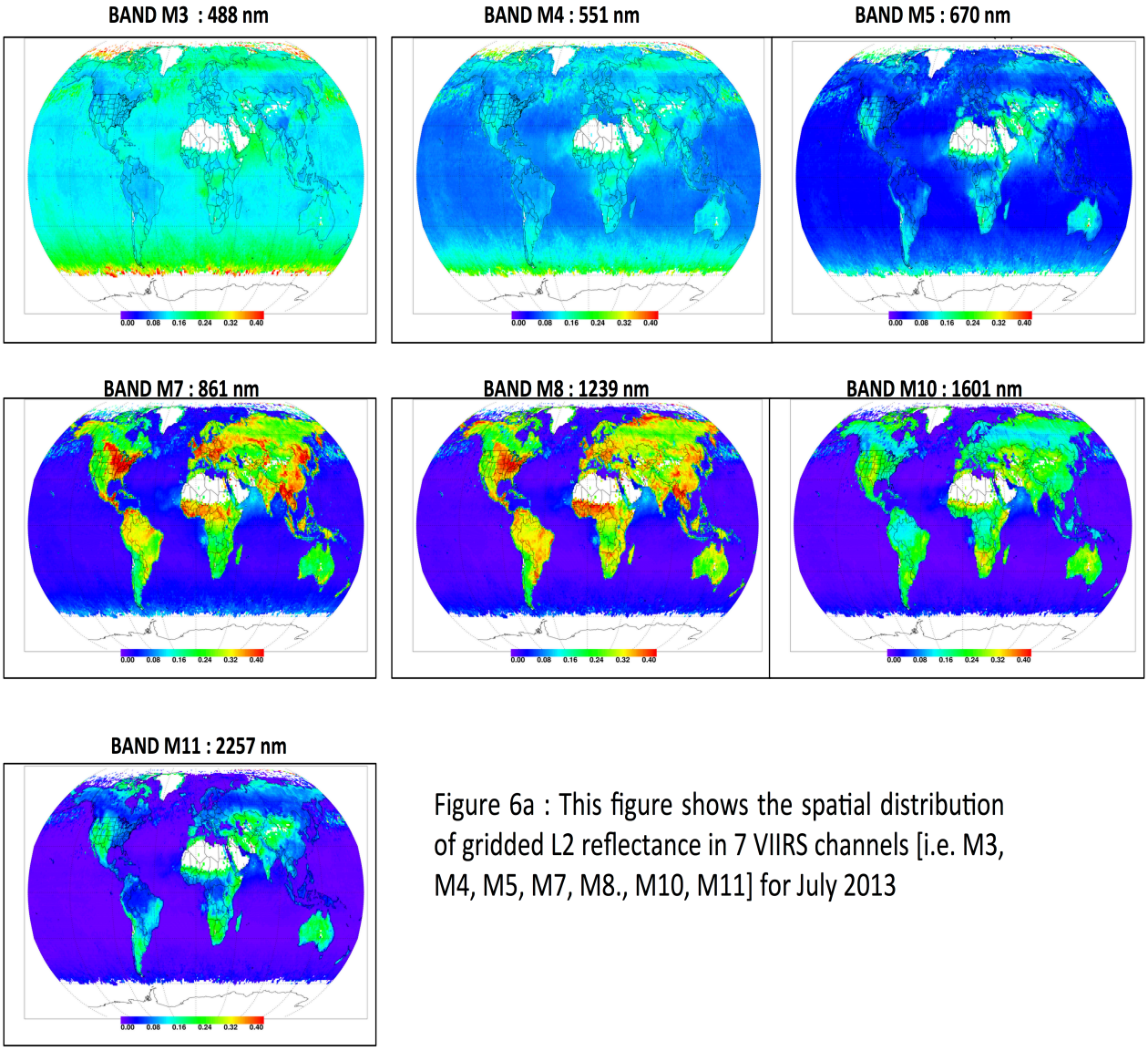

Figure 6a : This figure shows the spatial distribution of gridded L2 reflectance in 7 VIIRS channels [i.e. M3, M4, M5, M7, M8., M10, M11] for July 2013

822
823

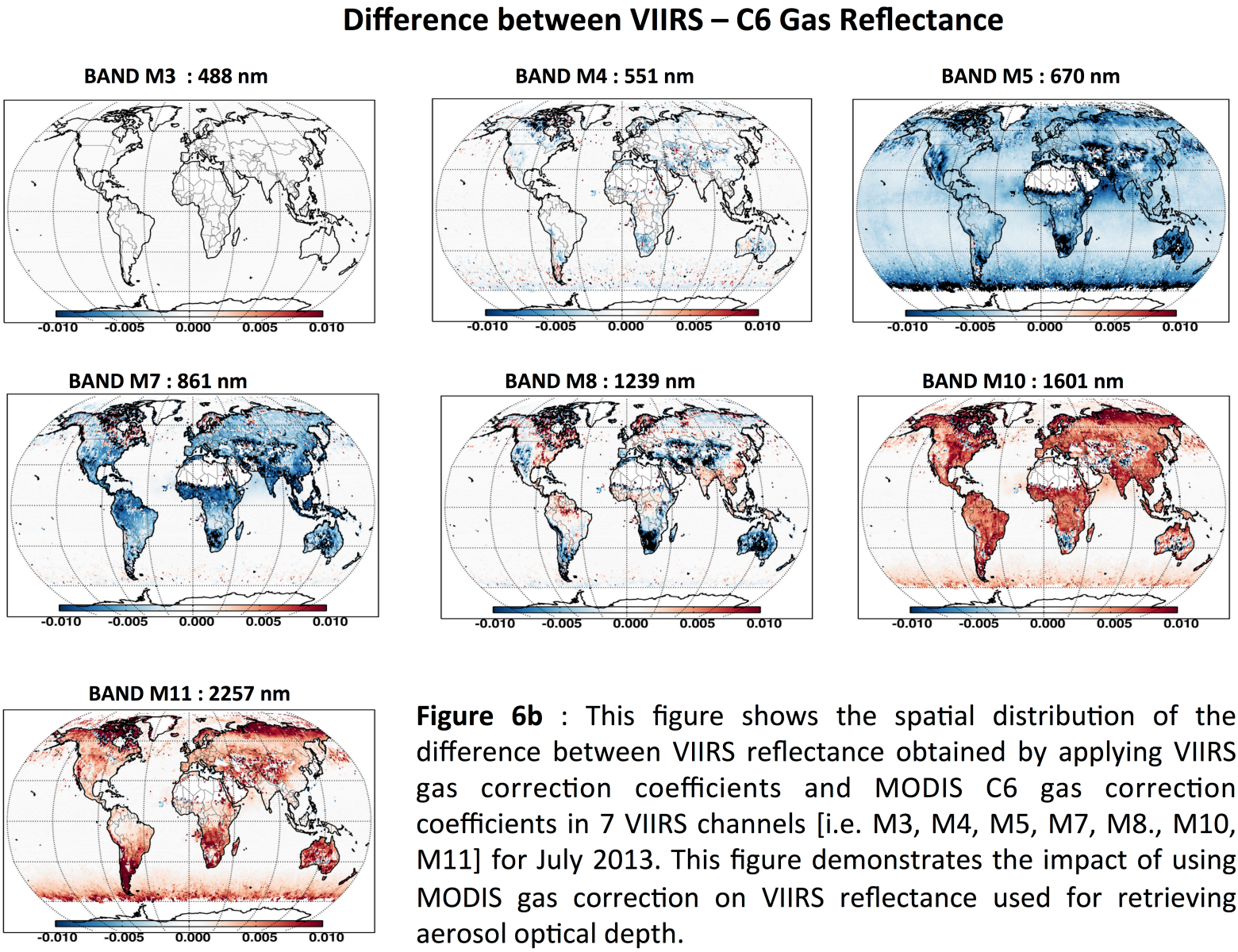

Figure 6b : This figure shows the spatial distribution of the difference between VIIRS reflectance obtained by applying VIIRS gas correction coefficients and MODIS C6 gas correction coefficients in 7 VIIRS channels [i.e. M3, M4, M5, M7, M8., M10, M11] for July 2013. This figure demonstrates the impact of using MODIS gas correction on VIIRS reflectance used for retrieving aerosol optical depth.

824
825
826
827
828
829
830
831
832
833

834

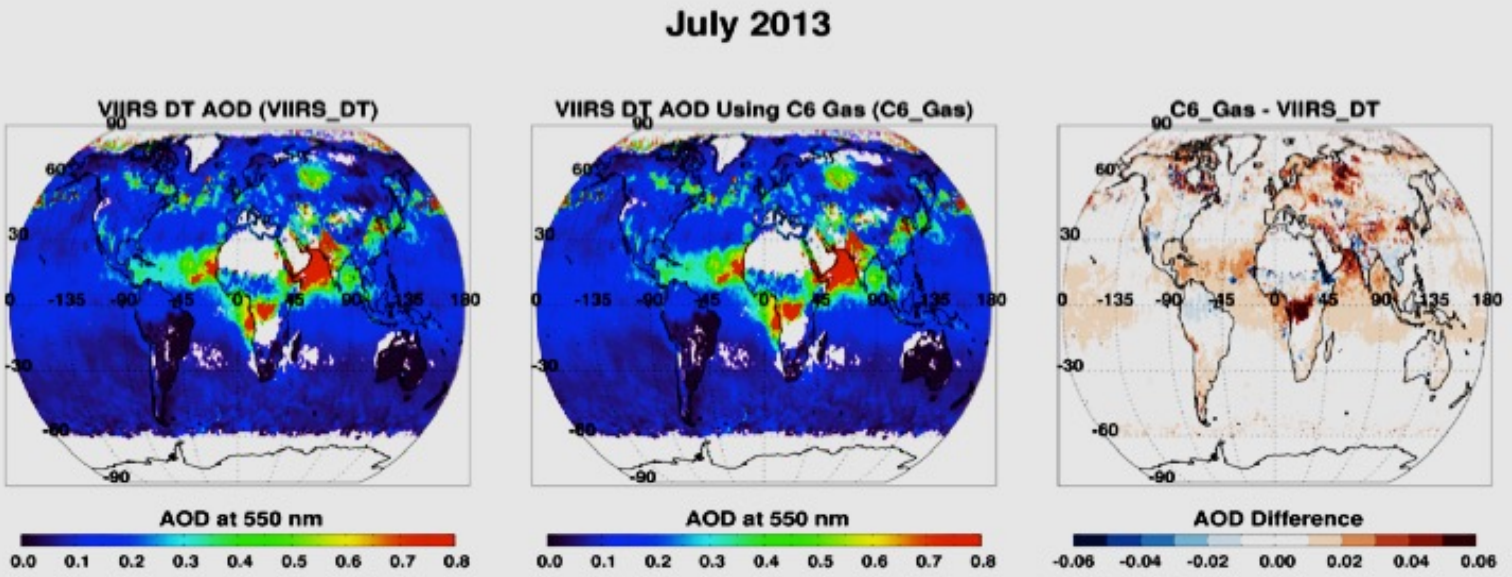

Figure 7: Impact of updated atmospheric corrections on VIIRS AOD (550 nm) retrieval. All things being equal, using C6 aerosol DT retrieval algorithm (a) is AOD using atmospheric coefficients calculated for VIIRS bands and (b) is AOD using C6 atmospheric corrections (c) is the difference between (b) and (a). The global mean AOD differs by ~0.012 over land and by ~0.004 over ocean. Difference are larger than these mean values regionally but <0.08. Differences are mostly positive (reds) except in some desert / bright regions where some negative differences appear.

835
836
837
838
839
840
841
842
843
844
845
846
847
848

Tables

Table 1 : Absorption bands of atmospheric gases in visible and near-IR region

Major Atmospheric Gas	Center Wavelengths (μm)
H_2O	visible, 0.72, 0.82, 0.94, 1.1 1.38, 1.87, 2.7
CO_2	1.4, 1.6, 2.0, 2.7, 4.3
O_3	visible (0.45 - 0.75)
O_2	0.63, 0.69, 0.76, 1.06, 1.27, 1.58
N_2O	2.87, 4.06, 4.5
CH_4	1.66, 2.2, 3.3
CO	2.34, 4.67
NO_2	visible

887

Table 2.1 : Optical depth of major atmospheric gases in 7 MODIS channels.

888
889
890

Channel	B3	B4	B1	B2	B5	B6	B7
Wavelength (µm)	0.466	0.553	0.645	0.856	1.242	1.638	2.113
Gas							
H2O	0.0001	0.0005	0.0055	0.0086	0.005	0.0017	0.0254
O3	0.0029	0.0326	0.0250	0.0008	-	-	0.0000
CO2	-	-	-	-	0.0003	0.0050	0.0142
N2O	-	-	-	-	-	-	0.0020
CO	-	-	-	-	-	-	-
O2	0.0012	0.0010	0.0038	0.0000	0.0164	-	-
NO	-	-	-	-	-	-	-
SO2	-	-	-	-	-	-	-
NO2	-	-	-	-	-	-	-
CH4	-	-	-	-	0.0000	0.0051	0.0003
Total	0.0042	0.0341	0.0344	0.0094	0.0216	0.0118	0.0420

891
892

Highlighted boxes show channels where total gas optical depth ≥0.02 to put in context the requirement of aerosol optical depth accuracy of better than 0.02

893
894
895

896

Table 2.2 : Optical depth of major atmospheric gases in 7 VIIRS channels

897

Channel Gas	M3	M4	M5	M7	M8	M10	M11
Wavelength (µm)	0.488	0.551	0.67	0.861	1.239	1.601	2.257
Gas							
H2O	0.00009	0.00078	0.00066	0.00324	0.00844	0.00234	0.00542
O3	0.00673	0.0312	0.01499	0.00075	0	0	0
CO2	0	0	0	0	0.00041	0.02048	0.00001
N2O	0	0	0	0	0	0.00001	0.00403
CO	0	0	0	0	0	0	0
O2	0.00184	0.00084	0.00144	0.00002	0.01147	0	0
NO	0	0	0	0	0	0	0
SO2	0	0	0	0	0	0	0
NO2	0	0	0	0	0	0	0
CH4	0	0	0	0	0.00001	0.00085	0.04914
Total	0.00866	0.03282	0.01709	0.00401	0.02033	0.02368	0.0586

898
899

Highlighted boxes show channels where total gas optical depth ≥0.02 to put in context the requirement of aerosol optical depth accuracy of better than 0.02

900
901
902
903
904
905

Table 3.1: Gas Absorption Coefficients and Climatology for MODIS

MODIS Band	Wavelength (μm)	Rayleigh Optical Depth	O_3 Optical Depth#	H_2O Optical Depth#	Dry Gas* Optical Depth#	O_3_K0	O_3_K1	H_2O_K0	H_2O_K1	H_2O_K2
B3	0.4659	1.92E-01	2.90E-03	8.00E-05	1.25E-03	-1.14E-04	8.69E-06	-9.58E+00	1.23E+00	-1.16E-01
B4	0.5537	9.44E-02	3.26E-02	5.00E-04	9.50E-04	5.18E-06	9.50E-05	-7.91E+00	1.00E+00	-1.29E-02
B1	0.6456	5.08E-02	2.52E-02	5.11E-03	3.91E-03	1.16E-04	7.32E-05	-5.60E+00	9.40E-01	-1.78E-02
B2	0.8564	1.62E-02	8.10E-04	8.61E-03	2.00E-05	2.80E-07	2.36E-06	-5.07E+00	8.77E-01	-2.40E-02
B5	1.2417	3.61E-03	0.00E+00	5.23E-03	1.69E-02	1.19E-07	1.55E-25	-5.65E+00	9.81E-01	-2.38E-02
B6	1.6285	1.22E-03	0.00E+00	1.62E-03	9.98E-03	1.19E-07	5.17E-26	-6.80E+00	1.03E+00	-4.29E-03
B7	2.1134	4.30E-04	2.00E-05	2.53E-02	1.63E-02	6.29E-07	7.03E-08	-3.98E+00	8.86E-01	-2.56E-02

* Dry Gas includes CO_2, CO, N_2O, NO_2, NO, CH_4, O_2, SO_2

For each MODIS band, this nadir looking (viewing zenith angle = 0) optical depth for the gas is computed from the US 1976 Standard Atmosphere in LBLRTM.

Table 3.2: Gas Absorption Coefficients and Climatology for VIIRS

VIIRS Band	Wavelength (μm)	Rayleigh Optical Depth	O_3 Optical Depth#	H_2O Optical Depth#	Dry Gas* Optical Depth#	O_3_K0	O_3_K1	H_2O_K0	H_2O_K1	H_2O_K2
M3	0.488	1.60E-01	6.73E-03	8.94E-05	1.84E-03	-1.25E-04	1.98E-05	-9.65E+00	9.87E-01	1.80E-04
M4	0.5511	9.76E-02	3.11E-02	7.69E-04	8.34E-04	-4.75E-05	9.08E-05	-7.50E+00	9.84E-01	-3.87E-03
M5	0.6704	4.40E-02	1.50E-02	6.64E-04	1.44E-03	-4.79E-05	4.37E-05	-7.69E+00	9.95E-01	-1.10E-02
M7	0.8612	1.60E-02	7.70E-04	3.37E-03	2.45E-05	4.18E-07	2.24E-06	-6.05E+00	9.65E-01	-1.53E-02
M8	1.2389	3.67E-03	0.00E+00	8.44E-03	1.19E-02	1.19E-07	5.17E-26	-5.16E+00	9.59E-01	-2.67E-02
M10	1.6012	1.32E-03	0.00E+00	2.34E-03	2.13E-02	1.19E-07	1.03E-25	-6.43E+00	1.02E+00	-3.60E-03
M11	2.257	3.50E-04	1.07E-06	5.42E-03	5.32E-02	-2.61E-08	3.28E-09	-5.85E+00	1.28E+00	-5.04E-03

* Dry Gas includes CO_2, CO, N_2O, NO_2, NO, CH_4, O_2, SO_2

For each VIIRS band, this nadir looking (viewing zenith angle = 0) optical depth for the gas is computed from the US 1976 Standard Atmosphere in LBLRTM.

Table 4: Atmosphere Gas Correction Table Differences : C5 vs C6

	C5	C6	Comment
RT Code	6s	LBLRTM (Line-by-Line Radiative Transfer Model)	6S is MODTRAN (Ref) database LBLRTM is HITRAN (Ref) database
# Gases Considered	3 [H2O, O3, CO2]	10 [H2O, O3,02, CO, CO2, CH4, NO,N2O,NO2, SO2]	Inclusion of 'other' dry gases in C6 created big differences in MODIS bands 5 & 7 (See Fig. 2)
Climatological GODs	Mid-latitude-Summer	US76 Standard Atmosphere	Ref

926